Bull Math Biol (2011) 73:2575–2604
DOI 10.1007/s11538-011-9637-5

ORIGINAL ARTICLE

From Inflammation to Wound Healing: Using a Simple Model to Understand the Functional Versatility of Murine Macrophages

Lauren M. Childs · Michael Paskow · Sidney M. Morris Jr. · Matthias Hesse · Steven Strogatz

Received: 5 August 2010 / Accepted: 27 January 2011 / Published online: 23 February 2011

Abstract Macrophages are fundamental cells of the innate immune system. Their activation is essential for such distinct immune functions as inflammation (pathogen-killing) and tissue repair (wound healing). An open question has been the functional stability of an individual macrophage cell: whether it can change its functional profile between different immune responses such as between the repair pathway and the

L.M. Childs (✉) · S. Strogatz
Center for Applied Mathematics, Cornell University, Ithaca, NY 14853, USA
e-mail: lmc74@cornell.edu

S. Strogatz
e-mail: shs7@cornell.edu

Present address:
L.M. Childs
School of Biology and School of Mathematics, Georgia Institute of Technology, Atlanta, GA 30332, USA

M. Paskow · M. Hesse
Department of Immunology, Cornell University, Ithaca, NY 14853, USA

M. Paskow
e-mail: mjp57@cornell.edu

Present address:
M. Paskow
ChanTest Corporation, Rockville, MD 20850, USA

Present address:
M. Hesse
Vertex Pharmaceuticals Inc, Cambridge, MA 02139, USA
e-mail: Matthias_Hesse@vrtx.com

S.M. Morris Jr.
Department of Microbiology and Molecular Genetics, University of Pittsburgh School of Medicine, Pittsburgh, PA 15219, USA
e-mail: smorris@pitt.edu

inflammatory pathway. We studied this question theoretically by constructing a rate equation model for the key substrate, enzymes and products of the pathways; we then tested the model experimentally. Both our model and experiments show that individual macrophages can switch from the repair pathway to the inflammation pathway but that the reverse switch does not occur.

Keywords Macrophage activation · Inflammation · Wound repair · Ordinary differential equation (ODE) model

1 Introduction

The mammalian immune system is responsible for maintaining homeostatic conditions within the body and ensuring survival of the host. A tightly controlled synergism between the two branches—innate and adaptive—of the mammalian immune system protects the host, while failure to establish or maintain homeostasis causes disease. Every successful immune response includes the detection of potential threats to the host, such as invading pathogenic organisms, induction of a sufficient inflammatory response to control or eliminate the threat, subsequent down regulation of the inflammatory response and finally repair of tissue damaged by the pathogen and the immune response.

Recent data demonstrate that populations of murine macrophages follow different activation pathways which elicit different physiological functions (Porcheray et al. 2005). However, the central question of how individual macrophages initiate along these different pathways remains unanswered. Can individual cells switch from a pathway that involves inflammation—killing invading pathogens and protecting the host—to a repair pathway—aiding wound healing (Porcheray et al. 2005; Stout and Suttles 2004; Reyes and Terrazas 2007)? Additionally, are there distinct macrophages within the population that are activated uniquely along one pathway or the other? Or does a change in functional direction require the exchange of local macrophage populations? In other words, the functional stability of individual macrophages is still largely unknown.

In this paper, we investigate through a simple mathematical model and biological experimentation the flexibility of individual macrophages activated under inflammatory and repair conditions.

1.1 Inflammation

Activation of the immune system initiates an inflammatory response, characterized by redness, swelling, heat and pain (Goldsby et al. 2002; Janeway et al. 2001). Any inflammatory response has to be flexible. While it is necessary to eradicate or control the invading pathogen, excessive damage to host tissue must be avoided. The immune response must adapt to changing conditions in the inflamed tissue as failure to do so will cause severe disease (Gause et al. 2003; Anthony et al. 2007). The regulatory mechanisms, which control and adjust immune responses, are still not well understood and are the object of intensive research efforts.

While most activated adaptive immune cells, such as T-cells, develop relatively stable functional profiles, which lead to the generation of immunological memory (Loehning et al. 2008), the stability or flexibility of activated macrophages has not been sufficiently investigated. The fact that macrophages do not generate an immunological memory response, in contrast to T-cells, suggests that these cells are flexible in their functional determination upon activation.

Macrophages are intimately involved in inflammation. They are essential for detecting invading pathogens and for tissue destruction. They attract and activate other immune cells, both innate and adaptive, by releasing small circulating proteins (cytokines and chemokines) and by presenting pathogen-derived antigens. They also actively destroy pathogens by phagocytosis. In addition to their role in the initial inflammatory response, they actively participate in the clearance of inflammation through uptake of tissue debris and dying immune cells. Finally, they participate in tissue repair and wound healing (Mosser and Edwards 2008).

1.2 Macrophage Biological Background

Monocytes, the precursors of macrophage and dendritic cells, derive from the haematopoietic stem cell. Two main types of macrophages, tissue-residing and circulating, exist. Before macrophages can perform any of their functions, they must be activated. Activation is induced by a variety of receptor-derived signals. Some of these receptors recognize commonly found signature molecules derived from pathogens, such as pathogen-associated molecular patterns (PAMPs), or from tissue damage, such as damage-associated molecular patterns (DAMPs), while others bind to specific cytokines, small circulating signaling proteins. Although there are a variety of types of macrophage activation, the two functional patterns of macrophages which have received the most extensive study and which we will consider in this paper are microbial-pathogen induced inflammation, known as classical activation (caMa or M1), and helminth-induced inflammation or tissue repair, known as alternative activation (aaMa or M2). These two functional patterns have traditionally been thought to be mutually exclusive, similar to the dichotomy in the profiles of T-helper effector T cells. It has previously been thought that a macrophage is either activated along the classical pathway or the alternative pathway, but not both (Gordon 2007).

The proper course of macrophage activation is essential for host survival. Dramatic changes in the outcome of an immune response due to macrophage activation were demonstrated in murine models of Schistosomiasis, a chronic inflammatory disease of humans in the tropics and subtropics, caused by persistent infections with trematode parasites. The invading parasite causes a moderate cytotoxic (T-helper-1 cytokine) dominated inflammatory immune response. When the mature female worm lays eggs there is a dramatic switch to humoral (T-helper-2 cytokine) inflammation in the infected host. Disease progression into the chronic stage is characterized by reduction of the inflammatory response (Pearce and MacDonald 2002). These changes are reflected in the activation pattern of macrophages. While initially most macrophages are activated along the inflammatory pathway, the ensuing change in cytokine response causes a dominant repair phenotype in the macrophage population at the site of original inflammation (Hesse et al. 2001; Fallon and Mangan 2007). Failure to

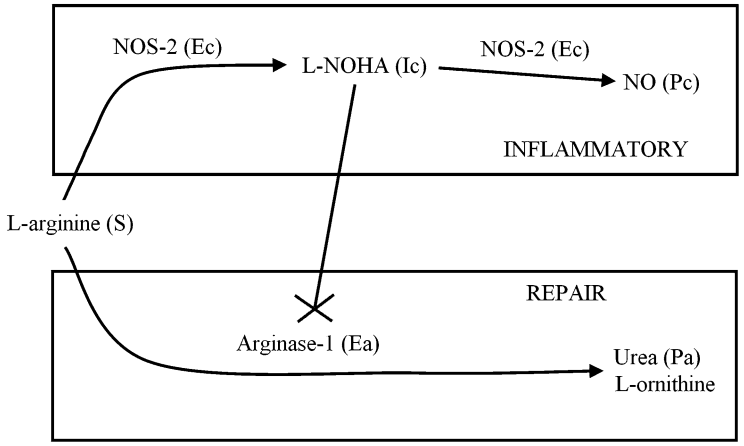

Fig. 1 Diagram of biological interactions of macrophage activation. The *top box* represents the Inflammatory or Classical Activation pathway. The *bottom box* represents the Repair or Alternative Activation pathway. The substrate, L-arginine (S), is used by both pathways. NOS-2 (E_C) is the enzyme of the inflammatory pathway. Arginase-1 (E_A) is the enzyme of the repair pathway. The products of the inflammatory pathway are nitric oxide (P_C) and L-citrulline, and the products of the repair pathway are urea (P_A) and L-ornithine (equimolar amounts). L-NOHA (I_C) is an intermediate of the inflammatory pathway and is involved in the inhibition of the enzyme of the repair pathway

change the functional phenotype of macrophages in the tissue from inflammatory to repair leads to massive tissue damage and subsequent death of the host (Herbert et al. 2004). A change in macrophage activation has also been reported during the inflammatory response against other parasites and in wound-healing models (Gordon 2003).

The dichotomy of L-arginine metabolism is one of the hallmarks of classical versus alternative macrophage activation (Gordon 2007; Modolell et al. 1995). Both pathways involve competition for the same substrate, L-arginine (Fig. 1). Inducible nitric oxide synthase (NOS-2) is the enzyme of the classical pathway and arginase-1 is the enzyme of the alternative pathway. The propensity toward either classical activation or alternative activation depends not only on the amount of each enzyme present in the cell but also on each enzyme's ability to bind sufficient substrate and the presence of inhibitors.

1.2.1 Classical Activation

Classical activation was discovered first, and for many years thereafter, was thought to be the only functional phenotype of macrophages during inflammation (MacMicking et al. 1997). Classical activation is induced by exposure to the cytokines Interferon-γ (IFN-γ) and Tumor Necrosis Factor-α (TNF-α) (Nathan 1994). Recognition of PAMPs, such as Lipopolysaccharide (LPS) or unmethylated cytosine and guanine (CpG) rich oligonucleotides, also induces classical activation of macrophages (Mosser 2003; Schreiber 1984; Stadecker et al. 2004). IFN-γ activates the Signal Transducers and Activation of Transcription (STAT)-1 signal transduction pathway

(Schreiber 1984) and thereby induces the expression of NOS-2. Substrate binding of L-arginine and O_2 with NOS-2 leads to the production of an intermediate, N-omegahydroxy-L-arginine (L-NOHA), which is ultimately metabolized into nitric oxide (NO) and L-citrulline (Stuehr 1999) (Fig. 1). NO is a free radical that has high toxicity to pathogens but also to host cells. Although most NO is utilized for the intracellular destruction of phagocytized microbes, caMa can release NO into the extracellular environment where it can harm not only pathogens but also neighboring cells. When self cells are damaged by NO, this is known as immune-mediated pathology (Bogdan 1997). Other features of classically activated macrophages are the production of various pro-inflammatory chemokines (e.g. CCL15, CCL20, CXCL10) and the T-helper-1 inducing cytokine IL-12 (Mosser and Edwards 2008).

Interaction between classical and alternative activation occurs with the intermediate, L-NOHA, formed during the production of NO (Hecker et al. 1995). L-NOHA preferentially binds the enzyme of the alternative pathway, arginase-1, and competitively inhibits the binding of arginase-1 to the substrate, L-arginine (Hecker et al. 1995; Boucher et al. 1994; Daghigh et al. 1994). This interaction establishes a relative dominance of the classical pathway over the alternative pathway because the intermediate of the classical pathway inhibits the enzyme of the alternative pathway (Fig. 1). Depending on the ratio of NOS-2 to arginase-1, we hypothesize that once the classical pathway has been initiated it is difficult to alter the activation state of a macrophage regarding arginine catabolism.

1.2.2 Alternative Activation

Although alternative activation of macrophages was first proposed 19 years ago (Stein et al. 1992), its importance was not immediately recognized. Today there is no doubt that aaMa have a central role in many aspects of inflammatory responses, such as chronic inflammation, atopies, fibrosis, maternal tolerance and immunity against infections (Martinez et al. 2008). Strictly defined, alternative activation refers to the response of macrophages to the cytokines interleukin-4 (IL-4) or interleukin-13 (IL-13) (Gordon and Martinez 2010). The cytokines interleukin-10 (IL-10) and interleukin-21 (IL-21) enhance alternative activation induced by IL-4 or IL-13 (Pesce et al. 2006). IL-4 and IL-13 induce the STAT-6 signal transduction pathway, leading to the up-regulation of arginase-1 expression. However, agents such as cyclic adenosine monophosphate (cAMP) also can induce arginase-1 in macrophages (Modolell et al. 1995; Morris et al. 1998); arginase-1 hydrolyzes L-arginine into L-ornithine and urea (Fig. 1). The arginase-1 reaction is considered to participate in tissue repair because it produces L-ornithine, which is a precursor for synthesis of polyamines (required for cell proliferation) and proline (required for synthesis of the proline-rich structural protein collagen). In hepatocytes arginase-1 is an essential enzyme of the urea cycle, which detoxifies ammonia in mammals (Wu and Morris 1998). Alternative activation of macrophages is also characterized by expression and release of proteins such as YM1 and RELMa, the cytokines CCL17, CCL22 and other factors contributing to wound healing (IGF1, Factor XIII-A) (Mosser and Edwards 2008).

As mentioned previously, L-NOHA, an intermediate of the classical pathway, binds arginase-1 and competitively inhibits binding of the substrate L-arginine to

arginase-1, effectively halting alternative activation. However, in the absence of L-NOHA, arginase-1 can bind and metabolize L-arginine, even at very low concentrations. Once arginase-1 is synthesized, its stability is independent of the presence or absence of its substrate, L-arginine. This is in contrast to NOS-2 which requires a minimum L-arginine presence and binding for formation of functional homodimers and to avoid rapid degradation (El-Gayar et al. 2003).

We hypothesize that a strong induction of NOS-2 expression will be sufficient to induce some minimum production of L-NOHA, which will increasingly inhibit the ability of arginase-1 to bind and metabolize L-arginine. This will enable individual macrophages to change from alternative to classical activation, as defined by the specific route of L-arginine catabolism.

As macrophages play an essential role in inflammation and tissue repair, understanding if individual macrophages can switch between the two pathways will significantly improve our understanding of immune responses and could help lead to design of new therapeutic strategies for a number of immune-mediated diseases.

2 Model Formulation

2.1 Modeling the Immune System

There have been many mathematical models of various aspects of the immune system—ranging from mechanistic to phenomenological. Models examine aspects from the intracellular dynamics through to the population dynamics, sometimes incorporating multiple levels. Some models focus on particular immune cells and others on particular pathogens. Using our model, we hope to address the role of the individual macrophage in flexibility of the functional direction of the macrophage population.

Wound healing and inflammation involving macrophages have previously been the subject of several mathematical studies (Waugh and Sherratt 2006; Maggelakis 2004, 2003; Pettet et al. 1996; Ourgrinovskaia et al. 2010; Marino et al. 2010; Wendelsdorf et al. 2010; Herald 2010; Shin et al. 2009; Marée et al. 2005). Most of these studies examine the dynamics of the population of macrophages as a whole, ignoring the individuals. In particular, the recent paper by Herald (2010) which examines the dynamics of macrophages in response to inflammatory and anti-inflammatory cytokines only examines the population level dynamics of the macrophages, not the behavior of individual macrophages. Further, models often focus on only one aspect of macrophage function—wound healing or inflammation.

We designed a model of the intracellular interactions of the substrate and enzymes involved with the L-arginine dichotomy within an individual macrophage. In the formulation of the model, an individual macrophage can enter both alternative and classical pathways, dependent on the presence or absence of particular cytokines.

We are well aware that alternative and classical activation states of macrophages involve changes in expression of genes other than arginase-1 and NOS-2. As we are considering only pathways of arginine catabolism, however, alternative or classical activation states in this study will be defined by cellular production of urea or NO, respectively.

2.2 Simplifying Assumptions

This model is not meant to be a completely accurate description of macrophage activation, but rather an incorporation of the key components of macrophage activation. There are six necessary simplifying assumptions we make during the formulation of the model which we describe below.

First, we assume that there is perfect signal transduction within the macrophage. In other words, given a particular cytokine signal, we assume that the corresponding enzymes are up-regulated to the fullest extent following a time course (sigmoidal curve over 50 hours) consistent with values published in the literature (Wei et al. 2000; Pauleau et al. 2004; Azenabor et al. 2009). Thus, the presence of IFN-γ determines the concentration of NOS-2 in the model and the presence of IL-4 determines the concentration of arginase-1 in the model.

Second, we assume that arginase-1 and NOS-2 act as standard enzymes in enzyme kinetics when they interact with L-arginine. That is, they reversibly form a substrate–enzyme complex before that complex irreversibly forms a product and releases the enzyme. This assumption allows us to write an ordinary differential equation (ODE) model of the system using Law of Mass Action kinetics.

Third, we assume only the enzymes degrade during the time course (50 hours) we are modeling. None of the other substances degrade appreciably or are present long enough to degrade on the time scale we are modeling. Thus, our equations only include terms for degradation for NOS-2 (E_{C}) and arginase-1 (E_{A}). Other terms in our equations, apart from the up-regulation described above, come directly from the Law of Mass Action description of our biological system.

Fourth, our model is completely deterministic. All of the substances considered appear in femtomolar quantities or larger within an individual cell, so there are at least 10^7 molecules per cell. This is a sufficient amount to ensure that in a well-mixed environment, which we assume here, chance does not affect the level of interactions.

Fifth, we assume a fixed amount of substrate, L-arginine, comparable to the amount available initially in each cell in our experiments. This amount of substrate is used during the reactions and is not replenished. Thus, we are not involving the cationic transporter system, which is responsible for transporting L-arginine from the extracellular matrix into the cell, nor the arginine biosynthetic enzymes that can convert L-citrulline to L-arginine. Further, we assume that O_2, the co-substrate for NOS-2, is not limiting for NO synthesis. Thus, the only limiting aspect is the amount of L-arginine.

Sixth, we assume that there is no feedback inhibition from the products to any part of the system. It is known that arginase-1 does cause feedback inhibition, but only under high substrate concentrations. However, our model looks at a regime of low substrate concentration with no replenishment.

2.3 Mathematical Formulation

The biology of the system can be written as four chemical kinetic equations as in (1). The subscripts C and A refer to molecules associated with the classical and alternative pathways, respectively. As the first three equations follow standard enzyme kinetics,

Table 1 Molecular components of macrophage activation

Type	Variable	Substance	Pathway
substrate	S	L-arginine	Both
enzyme	E_{C}	NOS-2	Classical
complex	$S : E_{\mathrm{C}}$	L-arginine:NOS-2 complex	Classical
intermediate	I_{C}	L-NOHA	Classical
complex	$I_{\mathrm{C}} : E_{\mathrm{C}}$	L-NOHA:NOS-2 complex	Classical
product	P_{C}	NO	Classical
enzyme	E_{A}	arginase-1	Alternative
complex	$S : E_{\mathrm{A}}$	L-arginine:arginase-1 complex	Alternative
product	P_{A}	L-ornithine	Alternative
inhibited enzyme	$I_{\mathrm{C}} : E_{\mathrm{A}}$	Inhibited arginase-1	Both
cytokine	C_{C}	IFN-γ	Classical
danger signal	A_{C}	CpG	Classical
cytokine	C_{A}	IL-4	Alternative
adjuvant	A_{A}	cAMP	Alternative

substrate–enzyme complexes (denoted with a colon between the substrate and the enzyme) are formed reversibly and are irreversibly turned into product, releasing the enzyme. The first equation, denoted $C1$, describes the formation of the classical intermediate, I_{C}, from the interaction of the substrate, S, with the classical enzyme, E_{C}. The second equation, denoted $C2$, describes the formation of the classical product, P_{C}, from the interaction of the classical intermediate, I_{C}, with the classical enzyme, E_{C}. $C1$ and $C2$ delineate the full classical pathway. The third equation, denoted $A1$, describes the formation of the alternative product, P_{A}, from the interaction of the substrate, S, with the alternative enzyme, E_{A}. The final equation, denoted $A2$, models the reversible inhibition of the alternative enzyme, E_{A} through interaction with the classical intermediate, I_{C}. The rate constants are denoted by the equation number and the direction: forward (F), reverse (R), or irreversible (IR). The biological name of the compounds described here are found in Table 1.

$$\begin{aligned}
C1\colon &\quad S + E_{\mathrm{C}} \underset{k_{C1\text{-}\mathrm{F}}}{\overset{k_{C1\text{-}\mathrm{R}}}{\rightleftarrows}} S : E_{\mathrm{C}} \xrightarrow{k_{C1\text{-}\mathrm{IR}}} E_{\mathrm{C}} + I_{\mathrm{C}} \\
C2\colon &\quad I_{\mathrm{C}} + E_{\mathrm{C}} \underset{k_{C2\text{-}\mathrm{R}}}{\overset{k_{C2\text{-}\mathrm{F}}}{\rightleftarrows}} I_{\mathrm{C}} : E_{\mathrm{C}} \xrightarrow{k_{C2\text{-}\mathrm{IR}}} E_{\mathrm{C}} + P_{\mathrm{C}} \\
A1\colon &\quad S + E_{\mathrm{A}} \underset{k_{A1\text{-}\mathrm{R}}}{\overset{k_{A1\text{-}\mathrm{F}}}{\rightleftarrows}} S : E_{\mathrm{A}} \xrightarrow{k_{A1\text{-}\mathrm{IR}}} E_{\mathrm{A}} + P_{\mathrm{A}} \\
A2\colon &\quad I_{\mathrm{C}} + E_{\mathrm{A}} \underset{k_{A2\text{-}\mathrm{R}}}{\overset{k_{A2\text{-}\mathrm{F}}}{\rightleftarrows}} I_{\mathrm{C}} : E_{\mathrm{A}}
\end{aligned} \tag{1}$$

Classical activation involving the input of the cytokine, C_{C}, and enhancer, A_{C}, indicates the presence of the enzyme, E_{C}, the complexes, $S : E_{\mathrm{C}}$ and $I_{\mathrm{C}} : E_{\mathrm{C}}$, the

intermediate I_C, and the product P_C. Alternative activation involving the input of the cytokine, C_A, and enhancer, A_A, indicates the presence of the enzymes, E_A and $I_C : E_A$, the complex $S : E_A$, and the product P_A. These chemical equations were then written as a system of ten ODEs using Law of Mass Action kinetics. Additional terms were added to the equations of E_A and E_C to include induction of these enzymes with the presence of the appropriate signals. This induction has a sigmoidal form culminating at an asymptote of a maximum up-regulated level. Degradation terms were also added to the NOS-2 (E_C) and arginase-1 (E_A) equations.

Substrate:

$$\begin{aligned}\frac{d}{dt}S = &-k_{C1\text{-F}}SE_C + k_{C1\text{-R}}S : E_C \\ &- k_{A1\text{-F}}SE_A + k_{A1\text{-R}}S : E_A\end{aligned} \tag{2}$$

Classical:

$$\begin{aligned}\frac{d}{dt}E_C = &-k_{C1\text{-F}}SE_C + (k_{C2\text{-R}} + k_{C2\text{-IR}})I_C : E_C \\ &+ (k_{C1\text{-R}} + k_{C1\text{-IR}})S : E_C - k_{C2\text{-F}}E_C I_C \\ &+ \ F_C(t) - \gamma E_C\end{aligned} \tag{3}$$

$$\frac{d}{dt}S : E_C = k_{C1\text{-F}}SE_C - (k_{C1\text{-R}} + k_{C1\text{-IR}})S : E_C \tag{4}$$

$$\begin{aligned}\frac{d}{dt}I_C = &\ k_{C1\text{-IR}}S : E_C - k_{C2\text{-F}}E_C I_C + k_{C2\text{-R}}I_C : E_C \\ &- k_{A2\text{-F}}I_C E_A + k_{A2\text{-R}}I_C : E_A\end{aligned} \tag{5}$$

$$\frac{d}{dt}I_C : E_C = k_{C2\text{-F}}E_C I_C - (k_{C2\text{-R}} + k_{C2\text{-IR}})I_C : E_C \tag{6}$$

$$\frac{d}{dt}P_C = k_{C2_I\text{R}}I_C : E_C \tag{7}$$

Alternative:

$$\begin{aligned}\frac{d}{dt}E_A = &-k_{A1\text{-F}}SE_A + (k_{A1\text{-R}} + k_{A1\text{-IR}})S : E_A \\ &- k_{A2\text{-F}}I_C E_A + k_{A2\text{-R}}I_C : E_A \\ &+ F_A(t) - \gamma E_A\end{aligned} \tag{8}$$

$$\frac{d}{dt}S : E_A = k_{A1\text{-F}}SE_A - (k_{A1\text{-R}} + k_{A1\text{-IR}})S : E_A \tag{9}$$

$$\frac{d}{dt}P_A = k_{A1\text{-IR}}S : E_A \tag{10}$$

$$\frac{d}{dt}I_C : E_A = k_{A2\text{-F}}I_C E_A - k_{A2\text{-R}}\ I_C : E_A \tag{11}$$

where

$$F_{\mathrm{C}}(t) = G(C_{\mathrm{C}}, A_{\mathrm{C}}) \frac{M_{\mathrm{C}}\, t^{H_{\mathrm{C}}}}{\kappa_{\mathrm{C}}^{H_{\mathrm{C}}} + t^{H_{\mathrm{C}}}} \tag{12}$$

$$F_{\mathrm{A}}(t) = G(C_{\mathrm{A}}, A_{\mathrm{A}}) \frac{M_{\mathrm{A}}\, t^{H_{\mathrm{A}}}}{\kappa_{\mathrm{A}}^{H_{\mathrm{A}}} + t^{H_{\mathrm{A}}}} \tag{13}$$

where

$$G(C_{\mathrm{C}}, A_{\mathrm{C}}) = \begin{cases} 1 & C_{\mathrm{C}} > 0 \text{ and } A_{\mathrm{C}} > 0 \\ 0 & C_{\mathrm{C}} = 0 \text{ or } A_{\mathrm{C}} = 0 \end{cases} \tag{14}$$

$$G(C_{\mathrm{A}}, A_{\mathrm{A}}) = \begin{cases} 1 & C_{\mathrm{A}} > 0 \text{ and } A_{\mathrm{A}} > 0 \\ 0 & C_{\mathrm{A}} = 0 \text{ or } A_{\mathrm{A}} = 0 \end{cases} \tag{15}$$

Equations (12) and (13) describe the functional form of the input to the up-regulation of the enzymes. Equations (14) and (15) describe when (12) and (13) become non-zero in the presence of appropriate cytokines and adjuvants.

2.4 Rate Constants

Our model includes 19 rate constants. Unfortunately, few of these constants are measurable through experimentation. There exists, however, information from the literature about various rate constants.

Of the 19 rate constants in our model, we have explicit literature values for $k_{C2\text{-IR}}$, $k_{A1\text{-IR}}$, and γ_{C} (Mansuy and Boucher 2004; Alarcón et al. 2006; Kolodziejski et al. 2004). Additionally there exist literature values for $k_{C1\text{-IRrep}}$, $K_{C1\text{rep}}$, K_{C2}, K_{A1}, and K_i (Mansuy and Boucher 2004; Alarcón et al. 2006; Boucher et al. 1999; Moali et al. 1998, 2000; Santhanam et al. 2008). Literature values for the rate constants are found in Table 3.

2.5 Rate Constant Optimization

The explicit literature values for $k_{C1\text{-IRrep}}$, $k_{C2\text{-IR}}$, $k_{A1\text{-IR}}$, $K_{C1\text{rep}}$, K_{C2}, K_{A1}, and K_i (Mansuy and Boucher 2004; Alarcón et al. 2006; Boucher et al. 1999; Moali et al. 1998, 2000; Santhanam et al. 2008) provide information about relationships between $k_{C1\text{-F}}$, $k_{C1\text{-R}}$, $k_{C2\text{-F}}$, $k_{C2\text{-R}}$, $k_{A1\text{-F}}$, $k_{A1\text{-R}}$, $k_{A2\text{-F}}$ and $k_{A2\text{-R}}$ (Appendix A.1). The known information about the relationships of these constants is enough to severely restrict our choice of their values (Appendix A.1). As the choice of constants is robust over many scales, we have chosen values such that the reversible reactions and irreversible reactions proceed at equivalent rates, i.e. $k_{C1\text{-R}} = k_{C1\text{-IR}}$, $k_{C2\text{-R}} = k_{C2\text{-IR}}$, $k_{A1\text{-R}} = k_{A1\text{-IR}}$.

There exist no data on the explicit values describing the induction of the enzymes, such as the time to half induction of the enzymes and the Hill coefficients. However, there is data in the form of a "time to induction" curve of arginase-1 (E_{A}) (Wei et al. 2000). From this curve we estimated the time to half induction for arginase-1 (κ_{A}),

and noted the curve shows an up-regulation followed by a decline. A representative curve was achieved by assuming the enzymes were up-regulated to a maximal value via a sigmoidal curve and degraded proportional to their concentration. We estimated γ_A and H_A by comparison to a time to induction curve in the literature (Wei et al. 2000) (Fig. 8). We assumed that NOS-2 followed a similarly shaped curve. As NO, the product of NOS-2, is formed very quickly, we knew the enzyme must be up-regulated quickly. Additionally, the production of NO proceeds for long periods of time even though the half-life of NOS-2 is quite short. Thus, we determined κ_C and H_C where there was quick up-regulation of E_C but persistence over a long period (Fig. 8).

We optimized the remaining rate constants, M_C and M_A, by comparison to our simple experimental data. We varied the initial level of enzyme and found the parameters that most accurately described our data. First, we compared the model output to our basic experiments where we introduced varying initial levels of one enzyme, either NOS-2 (E_C) or arginase-1 (E_A) (experimental data from Fig. 3), and allowed the simulation to run for the equivalent of 50 hours. An increased level of NOS-2 (E_C) produced NO (P_C) but no urea (P_A), while an increased level of arginase-1 (E_A) produced urea (P_A) but no NO (P_C) (Fig. 9).

We also compared the model output to experiments where we introduced both enzymes simultaneously (experimental data from Fig. 4). When both enzymes were introduced together experimentally, a substantial level of NO (P_C) and not of urea (P_A), was produced. The classical activation overpowered alternative activation. However, in our model there is still an up-regulation of urea (Fig. 9). This discrepancy is likely because it is known that there are differing reaction rates with different ratios of the two enzymes (Santhanam et al. 2008). In the initial hours of this simulation, we significantly break the implicit assumption from our choice of constant rates of reactions that the molar ratio of NOS-2 to arginase-1 is near one. Instead, initially the level of NOS-2 is much higher than arginase-1 which would lead to a higher rate for NOS-2 and thus significantly less urea (Santhanam et al. 2008). The parameter values used in our simulations are found in Table 2.

3 Simulations

Simulations of our 10 ODE system were performed in Matlab using ode15s, a stiff-equation solver, with a variable step size.

In our simulations, we introduced both enzymes at separate time points during the 50 hour time course to examine how the products change in response to changes in the environment. In the first simulation, we initially introduced only arginase-1 (E_A) indicative of alternative activation. After 25 hours, we stopped the input of arginase-1 (E_A), removed the urea (P_A), and elevated the level of NOS-2 (E_C), indicative of classical activation. We continued the simulation for another 25 hours (total of 50 hours).

During the first 25 hours, the level of urea (P_A) became elevated (Fig. 2(b)). The amount of NO (P_C) produced in the final 25 hours after the introduction of NOS-2 (E_C) (Fig. 2(a)) was similar to that produced in the experiments with classical activa-

Table 2 Parameters of macrophage activation model

Parameter	Symbol	Value	Units
Rate of synthesis of $S : E_C$	$k_{C1\text{-F}}$	1.01×10^{10}	$h^{-1}\,mol^{-1}$
Rate of decomposition of $S : E_C$	$k_{C1\text{-R}}$	3.78×10^{5}	h^{-1}
Rate of synthesis of I_C	$k_{C1\text{-IR}}$	3.78×10^{5}	h^{-1}
Rate of synthesis of $I_C : E_C$	$k_{C2\text{-F}}$	1.35×10^{9}	$h^{-1}\,mol^{-1}$
Rate of decomposition of $I_C : E_C$	$k_{C2\text{-R}}$	2.70×10^{4}	h^{-1}
Rate of synthesis of P_C	$k_{C2\text{-IR}}$	2.70×10^{4}	h^{-1}
Rate of synthesis of $S : E_A$	$k_{A1\text{-F}}$	1.37×10^{9}	$h^{-1}\,mol^{-1}$
Rate of decomposition of $S : E_A$	$k_{A1\text{-R}}$	6.84×10^{5}	h^{-1}
Rate of synthesis of P_A	$k_{A1\text{-IR}}$	6.84×10^{5}	h^{-1}
Rate of synthesis of $I_C : E_A$	$k_{A2\text{-F}}$	7.2×10^{10}	$h^{-1}\,mol^{-1}$
rate of decomposition of $I_C : E_A$	$k_{A2\text{-R}}$	3.6×10^{6}	h^{-1}
Maximum induction of E_C	M_C	9×10^{-11}	mol
Maximum induction of E_A	M_A	4×10^{-11}	mol
Time to half induction of max E_C	κ_C	5	h
Time to half induction of max E_A	κ_A	25	h
Hill coefficient of E_C	H_C	1	N/A
Hill coefficient of E_A	H_A	4	N/A
Degradation rate of E_C	γ_C	0.433	h^{-1}
Degradation rate of E_A	γ_A	0.04	h^{-1}

tion as the only stimulus (Fig. 3(a)). The level of urea (P_A) became slightly elevated again at 48 hours (Fig. 2(b)), but not nearly to the magnitude seen with the single stimulation experiment via alternative activation (Fig. 3(b)). At the intermediate time point of 25 hours, we removed the product as it is in the supernatant and was washed away in the experiments.

In the second simulation, we first introduced only NOS-2 (E_C). After 25 hours we reset the input of NOS-2 (E_C), removed the NO (P_C), and elevated the level of arginase-1 (E_A). We then ran the simulation for another 25 hours (total of 50 hours). During the first 25 hours, the level of NO (P_C) was significantly elevated (Fig. 2(c)). Although the level of urea (P_A) became elevated during the final 25 hours (Fig. 2(d)), it was negligible compared to the level of NO (P_C) already created (Fig. 2(c), (d)). Additionally, there was a small production of NO (P_C) between 25 and 50 hours (Fig. 2(c)).

Our simulations indicated that it was possible to switch from alternative activation to classical activation (Fig. 2(a), (b)). However, the opposite switch, from classical activation to alternative activation, was not possible (Fig. 2(c), (d)).

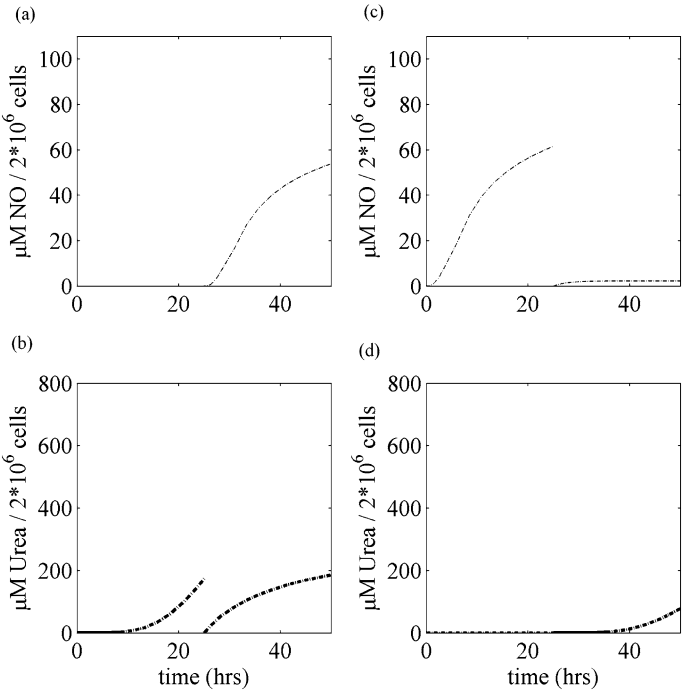

Fig. 2 Mathematical simulations of 10 ODE system. An initial condition per cell of $S = 5^{-10}$ M was used. All other initial conditions were zero. **a** Level of nitric oxide (P_C) and **b** level of urea (P_A) after alternative stimulation followed by classical stimulation. At the onset of the simulation the alternative enzyme (E_A) was up-regulated, analogous to the addition of IL-4 and cAMP in an experimental system. After 25 hours, the alternative enzyme input was removed along with the alternative product. At the same time, the input to the classical enzyme (E_C), analogous to the addition of IFN-γ and CpG experimentally, was included. **c** Level of nitric oxide (P_C) and **d** level of urea (P_A) after classical stimulation followed by alternative stimulation. At the onset of the simulation the classical enzyme (E_C) was up-regulated, analogous to the addition of IFN-γ and CpG in an experimental system. After 25 hours, the classical enzyme input was removed along with the classical product. At the same time, the input to the alternative enzyme (E_A), analogous to the addition of IL-4 and cAMP, was included

4 Experimental Results

We tested our mathematical model in biological experiments at the population and single cell level using the RAW 264.7 murine macrophage-like cell line. We exposed these cells to various stimuli. See Appendix A.3 for protocol.

In our experiments, we considered the presence of the classical product, NO, in the supernatant to be representative of the activation of the classical pathway. To stimulate the classical pathway, we exposed the macrophages to the cytokine IFN-γ and enhanced the stimulation with immunostimulatory CpG oligonucleotides (Krieg 2000). Alternative activation was determined by urea production after stimulation with IL-4 and cAMP.

This initial approach did not allow detection of the activation profile of single cells. Therefore we employed transfected RAW 264.7 cells with the gene for green fluorescent protein (GFP) under control of the arginase-1 promoter. Whenever a sig-

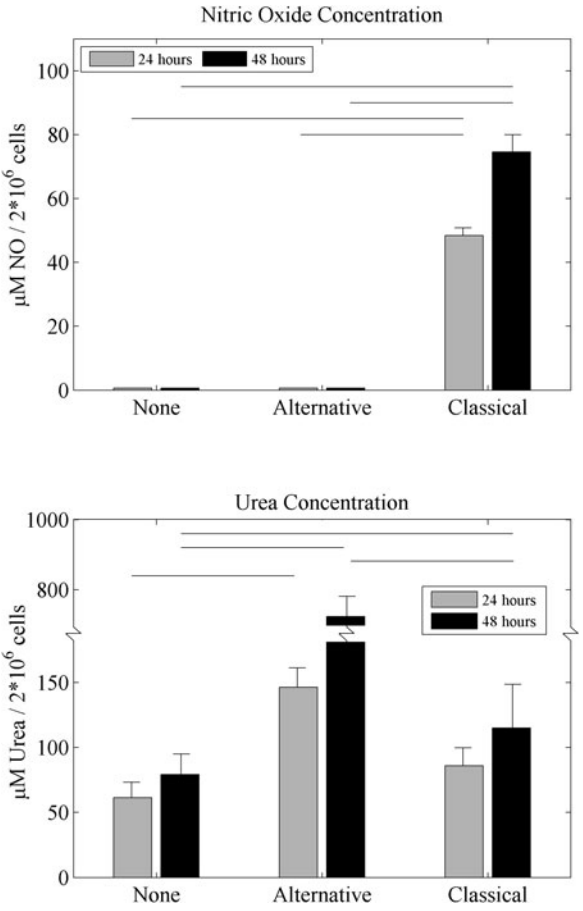

Fig. 3 Population level experimental data, single stimulation. **a** Nitric oxide concentration and **b** urea concentration after exposure of RAW 264.7 murine macrophages at time 0 to: only medium (*far left*) indicating no stimulus; IL-4 + cAMP (*middle*) indicating alternative stimulus; and IFN-γ + CpG (*far right*) indicating classical stimulus. Concentrations were determined from the supernatant of 2×10^6 cells. *Gray bars* represent measurements at 24 hours. *Black bars* represent measurements at 48 hours. Each bar is representative of $n = 4$ experiments. *Lines at the top* of the plot stretching between bars represent a significant difference ($p < 0.01$) between the means using a t-test. The error bars show one standard deviation above the mean

naling event activated the arginase-1 promoter the cells up-regulated the expression of GFP in addition to arginase-1. The expression of GFP in individual cells could be detected by flow cytometry after excitation with laser light at 488 nm. By flow cytometry sorting we were able to isolate viable GFP+ and GFP− cells. Our approach allowed for the first time to investigate the activation profile of macrophages at the single cell level.

4.1 Functional Stability at the Cell Population Level

First, we investigated the functional stability of RAW 264.7 cells at the population level. Previous data indicated that caMa populations cannot be switched into aaMa but the reverse switch might be possible (Modolell et al. 1995; Rutschman et al. 2001). Our mathematical model made similar predications.

Initially we only stimulated one pathway at a time. IFN-γ and CpG were used together as the classical stimulus. IL-4 and cAMP were used together as the alternative stimulus. As expected, IFN-γ and CpG induced only production of NO (Fig. 3(a)),

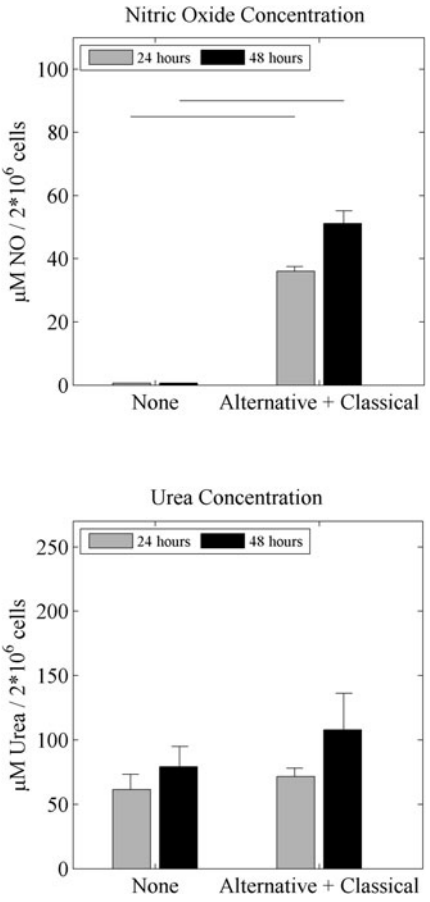

Fig. 4 Population level experimental data, double stimulation. **a** Nitric oxide concentration and **b** urea concentration after exposure of RAW 264.7 murine macrophages at time 0 to: only medium (*left*) indicating no stimulus; and IL-4 + cAMP + IFN-γ + CpG (*right*) indicating alternative stimulus and classical stimulus together. Concentrations were determined from the supernatant of 2×10^6 cells. *Gray bars* represent measurements at 24 hours. *Black bars* represent measurements at 48 hours. Each bar is representative of $n = 4$ experiments. *Lines at the top* of the plot stretching between bars represent a significant difference ($p < 0.01$) between the means using a t-test. No significant difference was found between any bars in **b**. The error bars show one standard deviation above the mean

but no urea (Fig. 3(b)). In contrast, stimulation with the IL-4 and cAMP generated urea production (Fig. 3(b)), but no NO (Fig. 3(a)).

We then considered the stimulation of both pathways at the same time, including both cytokines, IFN-γ and IL-4, as well as CpG and cAMP to enhance the signals. As predicted, the classical stimulus dominated, and only NO (Fig. 4(a)), not urea (Fig. 4(b)) was detected. These results are analogous to data from the literature in that simultaneous induction of NOS-2 and arginase-1 resulted in NO production but at a level that was less than if only NOS-2 was induced (Rutschman et al. 2001; Gotoh and Mori 1999).

Next, we investigated whether stimulation with one cytokine profile and the subsequent restimulation with the opposite cytokine profile could change the activation status of RAW 264.7 cells. We exposed cells to the classical stimulus, IFN-γ and CpG, and after 24 hours washed them and exposed them to the alternative stimulus, IL-4 and cAMP. These cells produced the classical product, NO, within the first 24 hours but only produced low amounts of NO (Fig. 5(a)) and no urea (Fig. 5(b)) upon restimulation along alternative activation. This low level of NO at the 48 hour time point should not be seen as a reduction of NO from the 24 hour time point. This

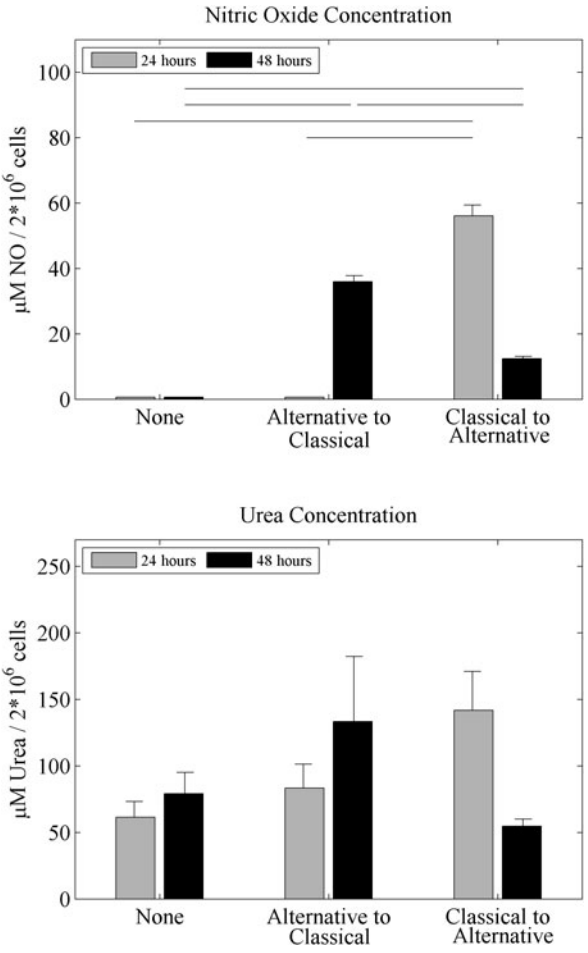

Fig. 5 Population level experimental data, sequential stimulation. **a** Nitric oxide concentration and **b** urea concentration after exposure of RAW 264.7 murine macrophages to: medium (*far left*) indicating no stimulus; IL-4 + CAMP (*middle*) indicating alternative stimulus at 0 hours followed by IFN-γ + CpG indicating classical stimulus at 24 hours; and IFN-γ + CpG (*far right*) indicating classical stimulus at 0 hours followed by IL-4 + cAMP indicating alternative stimulus at 24 hours. Cells were washed after 24 hours and before restimulation. Concentrations were determined from the supernatant of 2×10^6 cells. *Gray bars* represent measurements at 24 hours. *Black bars* represent measurements at 48 hours. Each bar is representative of $n = 4$ experiments. *Lines at the top* of the plot stretching between bars represent a significant difference ($p < 0.01$) between the means using a t-test. No significant difference was found between any bars in **b**. The error bars show one standard deviation above the mean

is an additional small production of NO after the washing of the cells. This increase is significantly less than the increases seen between 24 and 48 hours when there is only classical stimulation (Fig. 3(a)) or when there is both classical and alternative stimulation (Fig. 4(a)). As none of the urea concentrations are significantly different from that observed in the control (Fig. 5(b)) either at 24 or 48 hours, we cannot report any increased production of urea.

Additionally we performed the opposite switch and exposed cells to the alternative stimulus, IL-4 and cAMP, and after 24 hours washed them and exposed them to the classical stimulus, IFN-γ and CpG. After the initial 24 hours, neither NO nor urea was detected in significant amounts (Fig. 5(a)–(b)). Although the small amount of urea was similar to what was seen after 24 hours with the single stimulus experiments, it was not significantly different from the control. This is in contrast to the significant difference found in the single stimulation experiments (Fig. 3(b)). However, after restimulation with the classical stimulus, the cells produced NO (Fig. 5(a)). These

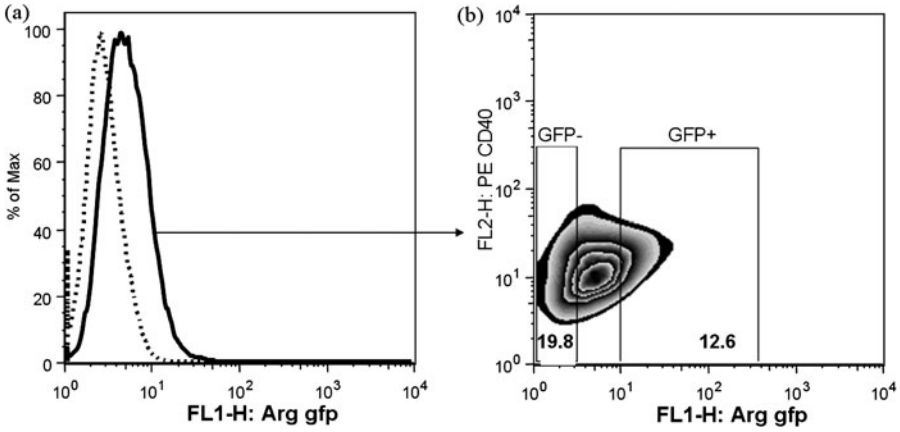

Fig. 6 Up-regulation of arginase-1 GFP after alternative stimulation. RAW 264.7 macrophages were stimulated alternatively with IL-4 + cAMP. After 24 hours their fluorescence was measured on a FACS machine. **a** The x-axis represents GFP fluorescence from activation of the arginase-1 promoter and the y-axis represents the percentage of maximum fluorescence. The *dotted line* represents unstimulated cells. The *solid line* represents alternatively stimulated (IL-4 + cAMP) cells. **b** A contour plot showing the number of cells at varying levels of GFP fluorescence and PE CD40. The x-axis represents GFP fluorescence from activation of the arginase-1 promoter and the y-axis measures PE CD40, a marker of inflammation. The *boxes* show the gates used for GFP+ and GFP− populations during sorting. Cells with intermediate fluorescence were discarded

results indicate the ability of the population to switch from alternative activation to classical activation but not the reverse.

4.2 Functional Stability at the Single Cell Level

Although our previous results appear to support our mathematical model, the experimental approach described thus far could not exclude that the change in functionality resulted from the stimulation of different subpopulations rather than the switch of individual cells, as predicted in our model. We employed arginase-1-GFP reporter macrophages to investigate the functional flexibility of single cells.

As arginase-1 expression is associated with the alternative pathway of macrophage activation, we expected a significant up-regulation of GFP with the alternative stimulus, IL-4 and cAMP. As expected, there was a clear population-wide increase of GFP-mediated fluorescence (Fig. 6), concomitant with increased urea production (data not shown). Next, we sorted the cells 24 hours after the stimulation with IL-4 and cAMP into GFP-low and GFP-high expressing cells (Fig. 6(b)). Both populations were restimulated with IFN-g and CpG for 24 hours. Subsequently, both populations released NO into the supernatant, with a higher production by the GFP+ cells (Fig. 7). The NO production by GFP+ cells demonstrates that individual macrophages can change from alternative to classical activation.

4.3 Comparison of the Model and Experiments

Although our model qualitatively predicts the switch of individual macrophages from alternative activation to classical activation, we need to quantitatively examine the

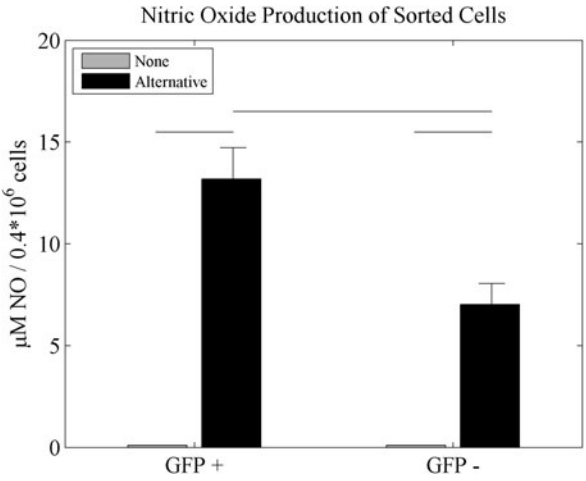

Fig. 7 Single cell level experimental data, GFP+ vs. GFP−. RAW 264.7 macrophages were stimulated alternatively with IL-4 + cAMP. After 24 hours they were sorted using a FACS machine based upon their expression of GFP, a marker for arginase-1 promoter, as GFP + (*left*) or GFP− (*right*). The sorted cells were washed and restimulated with medium or IFN-γ + CpG. The level of Nitric Oxide in the supernatant was measured after an additional 24 hours. *Gray bars* represent restimulation with medium. *Black bars* represent restimulation with IFN-γ + CPG. Each bar is representative of $n = 4$ experiments. *Lines at the top* of the plot stretching between bars represent a significant difference ($p < 0.01$) between the means using a t-test. The error bars show one standard deviation above the mean. *Note*: This experiment was performed with 0.4×10^6 cells rather than with 2×10^6 cells as in all other experiments, due to a low cell number after sorting

predictions. The results of our model are the amount of urea and NO produced by an individual cell under certain stimulation conditions. This is in contrast to our data which are reported for 2 million cells (Figs. 3–5) or 400,000 cells (Fig. 7). Thus, we expect the data in Figs. 3–5 to be 2×10^6 times greater than the model predictions. Similarly, the data in Fig. 7 are expected to be 4×10^5 times greater than the model predictions. We multiply our model results by 2×10^6 and express the result as the output per 2×10^6 cells for easier comparison to the data.

In the first simulation, where we initially introduced only arginase-1 (E_A) and subsequently at 25 hours reset the input of arginase-1 (E_A), eliminated the urea (P_A), and elevated the level of NOS-2 (E_C), we see only a small amount of production of urea at both the 25 and 50 hour time points (Fig. 2(b)). This is similar in magnitude but greater than what is seen at both time points from the data (Fig. 5(b)). During the final 25 hours, after the introduction of NOS-2 (E_C), the level of NO increased (Fig. 2(a)) to a slightly higher value than seen in the data (Fig. 5(a)).

In the second simulation, where we initially introduced only NOS-2 (E_C) and subsequently at 25 hours reset the input of NOS-2 (E_C), removed the NO (P_C), and elevated the level of arginase-1 (E_A), we see a similar production of NO and urea (Fig. 2(c), (d)) as seen in the experimental data at 25 hours (Fig. 5). At 50 hours, we see a small up-regulation of NO and urea (Fig. 2(c), (d)), both slightly below the level seen in the experimental data (Fig. 5).

Although not producing exact numerical values, our simulations were quantitatively close and accurately reproduced the trends of the data. Thus, our simulations

indicated that it was possible to switch from alternative activation to classical activation. However, the opposite switch, from classical activation to alternative activation, was not possible.

5 Discussion

Macrophages are highly versatile cells of the innate immune system (Mosser and Edwards 2008; Gordon 2003). Yet we still do not know how they adapt to different functional demands. Whether individual macrophages can change their functional profile or whether the exchange of cells in tissue leads to functional changes at the population level has not been fully understood. In the past, populations of cells were shown to change their functional phenotypes, both in vivo and in vitro (Mosser and Edwards 2008). It was never unequivocally determined whether individual cells were able to perform this switch.

We developed a 10 ODE mathematical model to make predictions regarding the functional flexibility of individual macrophages based on L-arginine metabolism in classically versus alternatively activated macrophages.

As we were interested in the short term dynamics of the model (see Appendix A.2), on the same time scale as experiments, we examined simulations of our mathematical model. Our simulations predicted the ability of an individual macrophage to switch from alternative activation to classical activation when the environmental conditions switched from alternative to classical and when there is single, non-replenishable pool of substrate. The reverse switch from classical activation to alternative activation was not observed.

Then we tested our mathematical predictions using RAW 264.7 cells. These cells were stimulated in vitro to induce classical or alternative activation of macrophages. We used the metabolic products of NO from NOS-2 and urea from arginase-1 as indication of each activation pathway. We found that classical activation was dominant over alternative activation at the population level. Simultaneous or consecutive stimulation caused NO production but did not result in significant urea production. These data are in accordance with previous results (Rutschman et al. 2001; Gotoh and Mori 1999) and they are consistent, both qualitatively and quantitatively, with our mathematical predictions.

Next, we investigated the functional flexibility of individual aaMa using our GFP-reporter cell line. Our results demonstrate the ability of individual aaMa to develop a classical phenotype of NO production. It argues against a model where the phenotypic switch at the population level is mediated by a response of different subpopulations to the various stimuli. In support of this finding, a recent study in an atherosclerosis model concluded that a local switch from alternative to classical macrophage activation in the inflammatory lesions is due to the conversion of cells already present and does not require the infiltration of new macrophages (Khallou-Laschet et al. 2010). However, this report did not exclude the possibility of switching local macrophages with different phenotypes.

As noted by Santhanam et al. (2008) the ratio of enzymes as well as the level of substrate, L-arginine, have an effect on the activity of the enzymes. Compared to their work, our simulations and experiments are almost always in a low L-arginine

regime and with a NOS-2/arginase-1 ratio near unity when both enzymes are present. According to Santhanam et al. (2008) this implies a similar but slightly higher activity for arginase-1 over NOS-2. The one exception, as noted, is when both classical and alternative stimulation are given concurrently. Then the ratio of NOS-2 to arginase-1 is large so NOS-2 should have a higher activity (Santhanam et al. 2008). The standard relative differences in activity are reflected in our choice of rate constants.

5.1 Pathway Priming

To ensure in-vivo-like conditions for our model, a danger signal by immunostimulatory CpG-oligonucleotides was part of our classical activation of RAW 264.7 cells in conjunction with IFN-γ. As expected, this classical stimulus caused the cells to up-regulate NO production, while the activity of arginase-1 was not elevated above background level (Fig. 4).

To our surprise however, many cells also started to express GFP as an indication of the activation of the arginase-1 promoter (data not shown). Neither IFN-γ nor CpG alone induced any significant GFP-expression.

It seems, co-stimulation of the cells by IFN-g and CpG changes the phenotype of these macrophages by priming them for potential alternative activation. Recently it was reported that Toll-like-Receptor-(TLR)-activation can induce arginase-1 expression in murine macrophages independent of STAT-6 activation. This can compromise their ability to control some intracellular microbial pathogens by interfering with the production of NO (El Kasmi et al. 2008). The study did not provide evidence for a complete change in phenotype from classical to alternative activation through the production of urea. In contrast our classically-restimulated alternative macrophages had a complete change of phenotype as seem by production of NO (Fig. 7). Therefore it seems that expression of arginase-1 under highly inductive classical conditions serves mainly to control excessive NO-mediated tissue damage.

Nevertheless, we cannot exclude that under certain conditions some macrophages will eventually be able to turn off classical activation and become alternatively activated cells. However, we find it more likely that the majority of classically activated cells will perish due to activation-induced cell death, mainly caused by NO and TNF-α (Xaus et al. 2000).

Newly arriving macrophages will be activated at the inflammatory site. Particularly at later stages of the inflammatory response when the majority of classical stimuli, such as invading microbial pathogens, have been removed, new cells will develop an alternative phenotype and promote tissue restoration. We speculate that the change from classical to alternative activation of macrophages, as has been reported in wound-healing models (Albina et al. 1990), is achieved mainly at the population level and not by changing the phenotype of single cells. In support of our hypothesis, macrophages in a sterile wound model expressed preferentially alternative activation markers (Daley et al. 2010). In contrast, induction of classical activation in wound macrophages is largely dependent upon the presence of microbes (Mahoney et al. 2002).

Our mathematical and experimental data imply that individual macrophages keep their ability to switch to a classical-antimicrobial program. Obviously, this mechanism allows macrophages to react very fast to potentially dangerous situations for

the host such as re-occurrence of infectious microbes in wound tissue. On the other hand, the inability to switch single macrophages entirely from classical to alternative activation could avoid exploitation by microbial pathogens causing disarmament of macrophages. Clearly, certain pathogenic organisms are able to manipulate the L-arginine metabolism in macrophages and induce arginase-1 expression (El Kasmi et al. 2008).

There is no question that our mathematical and cultured cell models oversimplify the complex mechanisms of macrophage activation in vivo. Nevertheless, we demonstrate that it is possible to use mathematical models to successfully predict the response of these cells under specific conditions.

Macrophages are central for every function of the mammalian immune system, from surveillance and inflammation to tissue repair. Finding novel ways to manipulate their function and understand the limits and conditions for functional changes is essential for the development of treatment strategies for many diseases.

Acknowledgements We would like to thank Diane Kepka-Lenhart who created the arginase-1-GFP vector and the transfected RAW cells and also to thank the Cornell Flow Cytometry Core Facility. Our project was supported in part by an NSF Graduate Research Fellowship to L. Childs, by an NIH grant RO1GM57384 to S.M. Morris, Jr, and by an NSF grant CCF-0835706 to S. Strogatz.

Appendix

A.1 Parameter Determination

A.1.1 Rate Constants from Michaelis Menten Kinetics

Information on our reactions found in the literature comes from constants determined using Michaelis–Menten assumptions. Michaelis–Menten kinetics is a model of substrate–enzyme kinetics that assumes certain reactions occur significantly faster than other reactions. Analysis of Michaelis Menten models begins by using Law of Mass Action to write down a system of ODEs from chemical equations. For example, in the simplified system:

$$S + E \underset{k_{\mathrm{R}}}{\overset{k_{\mathrm{F}}}{\rightleftarrows}} C \xrightarrow{k_{\mathrm{IR}}} E + P$$

the substrate–enzyme system is comprised of a substrate (S), enzyme (E), complex (C), and product (P). Subsequently it is assumed that the amount of complex rapidly reaches equilibrium and remains there. Thus, the equations describing the dynamics of the complex are removed from the system of ODEs. Further, the total amount of enzyme (complexed C and uncomplexed E together) is considered to be constant which allows for additional simplifications. The above chemical equation can be summarized under Michaelis–Menten assumptions by the single rate equation:

$$\frac{dP}{dt} = k_{\mathrm{IR}} E_{\mathrm{total}} \frac{S}{K_{\mathrm{M}} + S} \tag{16}$$

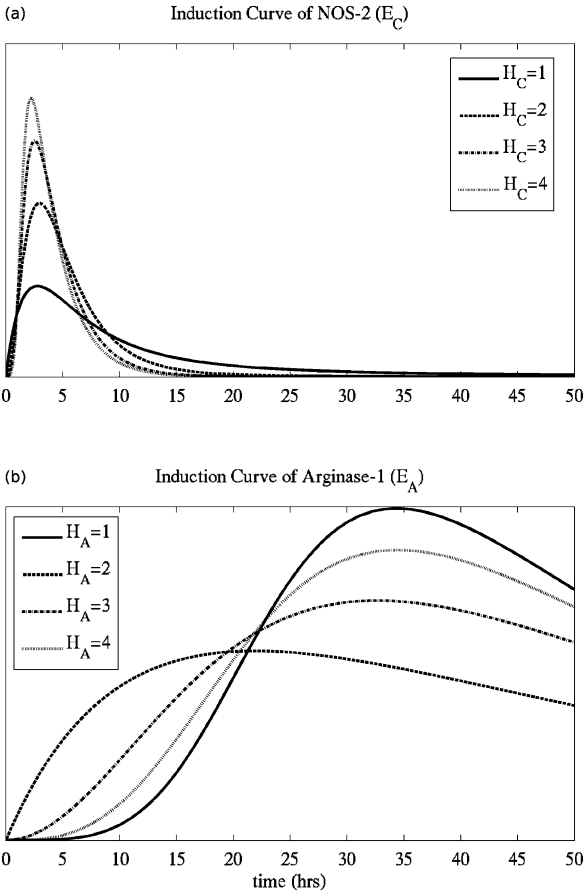

Fig. 8 Induction curves of enzymes. **a** The induction curve for NOS-2 (E_C) with varying values of the Hill coefficient, H_C. $H_C = 1$ described quick up-regulation of E_C and its persistence at low levels for the duration of the experiment. **b** The induction curve for arginase-1 (E_A) with varying values of the Hill coefficient, H_A. $H_A = 4$ and $\gamma_A = 0.04$ described initially slow up-regulation followed by persistence at high levels in the final hours of the experiment

where $K_M = \frac{k_{IR}+k_R}{k_F}$ is the Michaelis–Menten constant. Often in the literature the values of the rate constant at maximal rate and the substrate concentration when the rate is half maximal are reported. In this simple case, (16), k_{IR} is the rate constant at maximal rate and K_M is the substrate concentration when the rate is half maximal.

Further, it is understood how competitive inhibition, where a competing substrate molecule binds directly to the enzyme, seen in our model when L-NOHA binds arginase-1, affects the constants described above. For competitive inhibition k_{IR} remains the same while the Michaelis–Menten constant becomes $K_M(1 + \frac{C}{K_i})$. K_i is a measurable quantity and is directly related to the rate constants of the reaction involving the inhibition. For example, in our system $K_i = \frac{k_{A2\text{-R}}}{k_{A2\text{-F}}}$ gives us information of the ratios of $k_{A2\text{-R}}$ and $k_{A2\text{-F}}$.

Although the assumption of constant total enzyme does not hold for our system, the rate constants themselves should not be affected by the changing concentrations of complex and enzyme. Assuming a constant amount of enzyme, we can make the following assumptions from (2)–(11):

$$\frac{d}{dt}E_C + \frac{d}{dt}S : E_C + \frac{d}{dt}I_C : E_C = 0 \tag{17}$$

$$\frac{d}{dt}E_{\mathrm{A}} + \frac{d}{dt}S : E_{\mathrm{A}} + \frac{d}{dt}I_{\mathrm{C}} : E_{\mathrm{A}} = 0 \tag{18}$$

Considering only biologically relevant parameter sets, all intermediates and products have initial values of zero. Thus, $S : E_{\mathrm{C}}(0) = 0$, $I_{\mathrm{C}} : E_{\mathrm{C}}(0) = 0$, $S : E_{\mathrm{A}}(0) = 0$, and $I_{\mathrm{C}} : E_{\mathrm{A}}(0) = 0$. We integrate the above equations (17) and (18) and substitute in (2)–(11) for $E_{\mathrm{C}} = \bar{E}_{\mathrm{C}} - I_{\mathrm{C}} : E_{\mathrm{C}} - S : E_{\mathrm{C}}$ and $E_{\mathrm{A}} = \bar{E}_{\mathrm{A}} - I_{\mathrm{C}} : E_{\mathrm{A}} - S : E_{\mathrm{A}}$, where $\bar{E}_{\mathrm{C}}$ and $\bar{E}_{\mathrm{A}}$ are the total amount of classical or alternative enzyme, respectively, in any form. Further assume $\frac{d}{dt}S : E_{\mathrm{C}} = 0$, $\frac{d}{dt}I_{\mathrm{C}} : E_{\mathrm{C}} = 0$, $\frac{d}{dt}S : E_{\mathrm{A}} = 0$, and $\frac{d}{dt}I_{\mathrm{C}} : E_{\mathrm{A}} = 0$. Thus, our model becomes:

$$\frac{d}{dt}S = -\frac{k_{C1\text{-IR}}K_{C2}S}{I_{\mathrm{C}}K_{C1} + (S + K_{C1})K_{C2}}\bar{E}_{\mathrm{C}} - \frac{k_{A1\text{-IR}}S}{S + (\frac{I_{\mathrm{C}}}{K_i} + 1)K_{A1}}\bar{E}_{\mathrm{A}} \tag{19}$$

$$\frac{d}{dt}I_{\mathrm{C}} = \frac{k_{C1\text{-IR}}K_{C2}S - k_{C2\text{-IR}}K_{C1}I_{\mathrm{C}}}{I_{\mathrm{C}}K_{C1} + (S + K_{C1})K_{C2}}\bar{E}_{\mathrm{C}} \tag{20}$$

$$\frac{d}{dt}P_{\mathrm{C}} = \frac{k_{C2I_{\mathrm{R}}}K_{C1}I_{\mathrm{C}}}{I_{\mathrm{C}}K_{C1} + (S + K_{C1})K_{C2}}\bar{E}_{\mathrm{C}} \tag{21}$$

$$\frac{d}{dt}P_{\mathrm{A}} = \frac{k_{A1\text{-IR}}S}{S + (\frac{I_{\mathrm{C}}}{K_i} + 1)K_{A1}}\bar{E}_{\mathrm{A}} \tag{22}$$

where $K_{C1} = \frac{k_{C1\text{-IR}} + k_{C1\text{-R}}}{k_{C1\text{-F}}}$, $K_{C2} = \frac{k_{C2\text{-IR}} + k_{C2\text{-R}}}{k_{C2\text{-F}}}$, and $K_{A1} = \frac{k_{A1\text{-IR}} + k_{A1\text{-R}}}{k_{A1\text{-F}}}$.

From these equations, we can immediately apply the literature values found for K_{C2}, K_{A1}, K_i, $k_{C2\text{-IR}}$, and $k_{A1\text{-IR}}$. However, for K_{C1} and $K_{C1\text{-IR}}$, our reactions are not as simple as (16). Since K_{C1} is the Michaelis–Menten constant of the production of P_{C} from S, the intermediate I_{C} is assumed to be at equilibrium. Thus, (19)–(22) simplify to the following when only the classical pathway is activated:

$$\frac{d}{dt}S = -\frac{\frac{k_{C1\text{-IR}}k_{C2\text{-IR}}}{k_{C1\text{-IR}} + k_{C2\text{-IR}}}S}{S + \frac{k_{C2\text{-IR}}}{k_{C1\text{-IR}} + k_{C2\text{-IR}}}K_{C1}}\bar{E}_{\mathrm{C}} \tag{23}$$

$$\frac{d}{dt}P_{\mathrm{C}} = \frac{\frac{k_{C1\text{-IR}}k_{C2\text{-IR}}}{k_{C1\text{-IR}} + k_{C2\text{-IR}}}S}{S + \frac{k_{C2\text{-IR}}}{k_{C1\text{-IR}} + k_{C2\text{-IR}}}K_{C1}}\bar{E}_{\mathrm{C}} \tag{24}$$

Thus, the reported values of the maximal rate and Michaelis–Menten constant are $K_{C1\mathrm{rep}} = \frac{k_{C2\text{-IR}}}{k_{C1\text{-IR}} + k_{C2\text{-IR}}}K_{C1}$ and $k_{C1\text{-IRrep}} = \frac{k_{C1\text{-IR}}k_{C2\text{-IR}}}{k_{C1\text{-IR}} + k_{C2\text{-IR}}}$.

The known information about the relationships of these constants is enough to severely restrict our choice of their values. We examined all combinations values of $k_{C1\text{-R}}$, $k_{C2\text{-R}}$, $k_{A1\text{-R}}$, and $k_{A2\text{-R}}$ such that $k_p = i \times 10^j$ where $p = [C1\text{-R}, C2\text{-R}, A1\text{-R}, A2\text{-R}]$, $i = 0, 1, \ldots, 9$, and $j = 0, \ldots, 8$ and found that unless the reverse reaction is significantly faster (at least 10^5 greater) than the irreversible reaction, any choice of our values does not change the output. Even at the very large

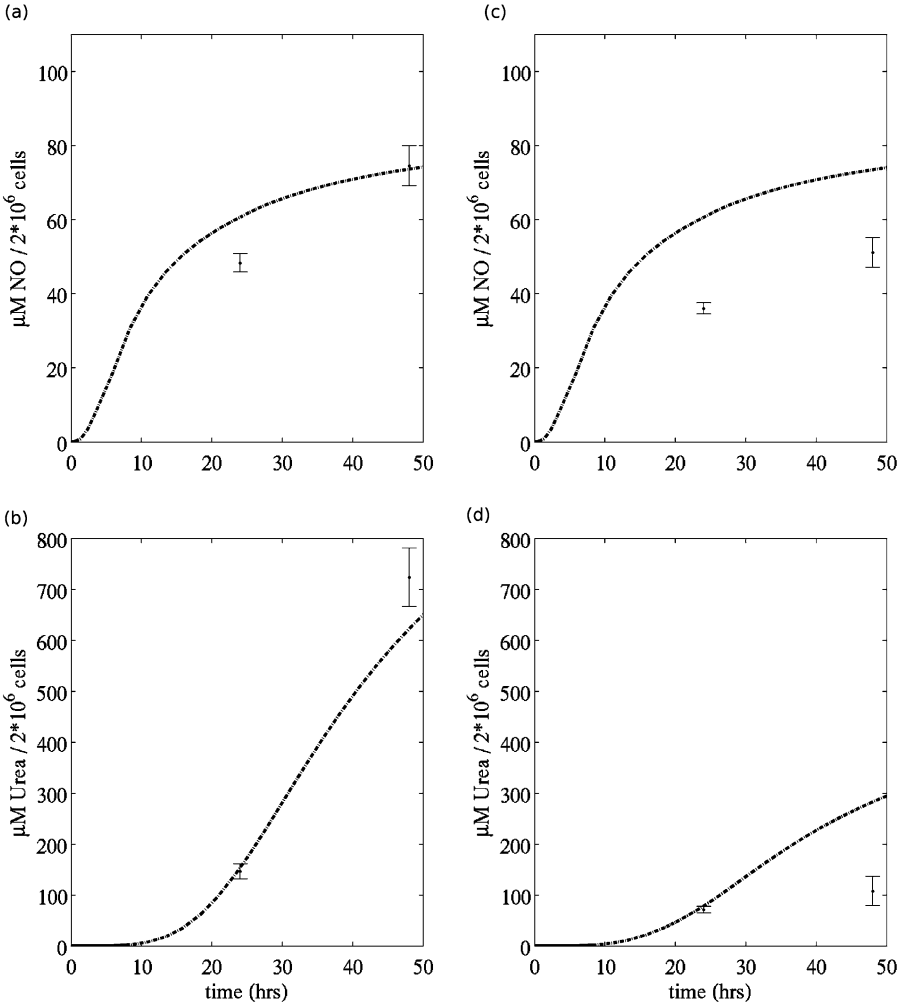

Fig. 9 Fitting of model to experimental data. The *curves* represent the model output while the dots represent experimental data with bars representing one standard deviation. The model results are multiplied by 2×10^6 to represent the output of 2 million cells, which is comparable to our experimental data. **a** NO concentration after classical stimulation with IFN-γ and CpG. Experimental data are from Fig. 3(a). **b** Urea concentration after alternative stimulation with IL-4 and cAMP. Experimental data are from Fig. 3(b). **c** NO concentration after classical and alternative stimulation with IFN-γ, CpG, IL-4 and cAMP. Experimental data are from Fig. 4(a). **d** Urea concentration after classical and alternative stimulation with IFN-γ, CpG, IL-4 and cAMP. Experimental data are from Fig. 4(b)

values of $k_{C1\text{-R}}$, $k_{C2\text{-R}}$, $k_{A1\text{-R}}$, and $k_{A2\text{-R}}$ the results only lower slightly. As the choice of constants is robust over many scales and we do not expect the reverse reaction to proceed so much (more than 10^5) faster than the irreversible reaction, we have chosen values such that the reversible reactions and irreversible reactions proceed at equivalent rates, i.e. $k_{C1\text{-R}} = k_{C1\text{-IR}}$, $k_{C2\text{-R}} = k_{C2\text{-IR}}$, $k_{A1\text{-R}} = k_{A1\text{-IR}}$.

Table 3 Literature values used to estimate parameters of model

Parameter	Symbol	Value	Units
MM constant of synthesis of P_C from S	$K_{C1\text{rep}}$	5×10^{-6} (Mansuy and Boucher 2004; Boucher et al. 1999)	mol
Rate of synthesis of I_C from S	$k_{C1\text{-IRrep}}$	2.4×10^{4} (Mansuy and Boucher 2004)	h^{-1}
MM constant of synthesis of P_C from I_C	K_{C2}	4×10^{-5} (Mansuy and Boucher 2004; Moali et al. 1998)	mol
Rate of synthesis of P_C from I_C	$k_{C2\text{-IR}}$	2.7×10^{4} (Mansuy and Boucher 2004)	h^{-1}
MM constant of synthesis of P_A from S	K_{A1}	1×10^{-3} (Alarcón et al. 2006; Santhanam et al. 2008)	mol
Rate of synthesis of P_A from S	$k_{A1\text{-IR}}$	6.8×10^{5} (Alarcón et al. 2006)	h^{-1}
Inhibition constant of E_A	K_i	5×10^{-5} (Moali et al. 2000)	mol
Degradation rate of E_C	γ_C	0.433 (Kolodziejski et al. 2004)	h^{-1}

A.2 Analysis of the Mathematical Model

To justify only considering the transient dynamics of our model, we also examined the asymptotic behavior of the system under a biologically relevant choices of parameters. We found the long term solution or fixed point of our equations by looking for solutions when all ten ODEs are equal to zero. To determine the stability of the fixed points we examine the eigenvalues of the Jacobian evaluated at our fixed point. Solving for the fixed points of the system, we find there is only one.

$$\begin{array}{ll} S = 0 & P_C = \text{unconstrained} \\ E_C = 0 & E_A = 0 \\ S : E_C = 0 & S : E_A = 0 \\ I_C = 0 & P_A = \text{unconstrained} \\ I_C : E_C = 0 & I_C : E_A = 0 \end{array}$$

The equilibrium values of the products P_C and P_A depend on the time course of intermediates, $I_C : E_C$ and $S : E_A$, respectively.

This fixed point is stable because the eigenvalues all have negative real parts except two which are zero. These two zero eigenvalues correspond to the P_C and P_A directions which we can ignore, because they do not feedback into the system. The remaining eight eigenvalues all have negative real parts. Thus the eigenvalues of the Jacobian lie in the left half plane indicating stability of our fixed point. The eigenvalues remain negative for all positive values of the rate constants, which constitutes the biologically relevant regime of parameters.

A.3 Experimental Protocol

Macrophage Activation Experimental Procedure

Production of RAW cells with a GFP transgene: A reporter murine macrophage-like cell line (RAW 264.7) was made for this project by transfecting the cells with

a plasmid containing the Green Fluorescence Protein (GFP) transgene driven by the 4.8 kb promoter for arginase-1 (Gray et al. 2005) within the vector pZsGreen-1-DR (Clontech; Mountain View CA). The vector also contains a neomycin-resistance cassette, which allows the transfected cells to be selected using G418. With this cell line, any time that the arginase-1 promoter is activated, GFP is also expressed. GFP, when struck by laser light, fluoresces and enables classification via flow cytometry. Once the cell line was received, the cells were stimulated and were sorted into GFP positive and negative cells and then selected for individual cell clones by limiting dilution. Cells were grown in DMEM high glucose without glutamine from BioWhittaker, Inc (Walkersville, MD) supplemented with 10 mL penicillin-streptomycin solution from GIBCO®, 10 mL 200 mM glutamine from BioWhittaker, Inc. (4 mM final), 5 mL 1 M HEPES from GIBCO® (15 mM final), 5 mL sodium pyruvate from GIBCO® and 50 mL defined Fetal Calf Serum (FCS) from HyClone (Logan, Utah; 10% final). All amounts are based upon 500 mL of DMEM. The concentration of L-arginine in complete DMEM is approximately 400 μM. Additionally G418 from A.G. Scientific, Inc. (San Diego, CA) at a concentration of 0.5 mg/mL was consistently added to the cells to select for those containing the transgene. The cells were incubated at 37°C in a 5% CO_2 and humidified environment.

Stimulation experiments: Using the RAW arginase-1/GFP cell clone D8, a number of stimulation experiments were performed. IL-4 from Cell Sciences (Canton, MA) and cAMP from Sigma-Aldrich (St. Louis, MO) in concentrations of 5 ng/mL and 0.5 mM, respectively, were used to induce alternative activation. IFN-γ from Cell Sciences at 100 units/mL or CpG ODN 1826 class B with the sequence 5′—TCCATGACGTTCCTGACGTT—3′ from Sigma-Genosys (The Woodlands, TX) at 1 μg/mL, which is an immunostimulatory oligonucleotide (23) that activates TLR9, and a combination of CpG and IFN-γ were used to induce classical activation. Stimulations were performed either in 24-well culture plates containing 1 mL of medium with 2 million cells per well (pre-sort experiments) or in 96-well culture plates containing 200 μL of medium with 400,000 cells per well (post-sort experiments).

Cell staining in preparation for flow cytometry analysis: The stimulated cells were incubated at 37°C for approximately 24 hours. Supernatants were saved in a 96-well titer plate and kept frozen at −20°C until they were tested for the presence of nitric oxide or urea. Cells were taken up in 1 mL of chilled phosphate buffer solution (PBS) from Mediatech, Inc. (Herndon, VA) and were incubated at 4°C for 10 minutes. Cells were then mixed with the PBS and transferred to separate FACS tubes. The tubes were centrifuged at 1200 rpm for 5 minutes, supernatants were discarded and 100 μL of a 1/200 dilution of PE-labeled anti-CD40 (final 0.02 mg/mL) from eBioscience, Inc. (San Diego, CA) in FACS buffer, consisting of PBS, 5 mg/mL Bovine Serum Albumin (BSA) form Fischer Scientific (Pittsburgh, PA) and 10% sodium azide, was added to each tube. CD40 is a surface protein, which functions as a co-stimulatory molecule for T- and B-cell activation. This protein is commonly used as a general marker for macrophage activation. Again the tubes were placed in 4°C to incubate for 15 minutes. 1 mL of FACS buffer was added to each tube, and the tubes were then placed back in the centrifuge for another 5-minute spin. The supernatants were

discarded and the cells were brought up in 300 μL of FACS buffer and were analyzed by flow cytometry on a FACS machine, FACSCalibur from BD (Franklin Lakes, NJ). The FACS machine was used to determine if there was an up-regulation of arginase-1/GFP in the stimulated cells. Analysis was performed using FlowJo version 4.6.2 and dead cells were excluded from the analysis by staining with 1 μL of 10 μg/mL stock solution of propidium iodide (PI) form Sigma-Aldrich, which invades only the leaky membranes of dead cells.

Analysis of supernatants for the production of nitric oxide by the Griess Reaction: Nitric oxide tests were performed (Hesse et al. 2000) using the supernatants that were removed from the activated cells and were then frozen. 50 μL of each sample were plated into a new 96-well titer plate with duplicates of each sample. Two rows were allocated for standards. 75 μL of the cell medium went into the first two wells and only 50 μL into the remaining. 25 μL of a 10 mM stock solution of sodium nitrite from Mallinckrodt Baker, Inc. (Paris, KY) was added to the first two wells and a serial dilution was performed down the row, leaving the last two wells alone as blanks; the extra 50 μL in the pipette was discarded. An equal amount of 'Solution A' consisting of sulfanilamide from Mallinckrodt Baker, Inc. at 1 mg/mL in 2.5% H_3PO_4 and 'Solution B' consisting of naphthylethylenediamine from Sigma-Aldrich at 3 μg/mL in 2.5% H_3PO_4 were mixed and 50 μL of the mixture was added to each well. The plate was then read at 543 nm on a PowerWave XS Microplate Scanning Spectrophotometer by Bio-Tek® Instruments, Inc. (Winooski, VT). The results were tabulated in Prism 4.0c by GraphPad Software, Inc. (San Diego, CA).

Analysis of supernatants for production of urea: Urea tests were performed (Munder et al. 1998) using the supernatants that were removed from the activated cells and were then frozen. 50 μL of each sample were transferred into 200 μL Eppendorf tubes. 50 μL of 50 mM $MnCl_2$-Tris solution—5 mL of $MnCl_2$ (0.989 g $MnCl_2$ in 50 mL water) plus 2.5 mL 1 M Tris plus 42.5 mL water—was added to each Eppendorf tube. The tubes were heated for 10 minutes in a 55°C water bath. 50 μL of each Eppendorf tube was transferred to a new 2 mL Eppendorf tube and placed on ice. 50 μL of 0.5 M arginine solution (0.871 g in 10 mL water) was quickly added to each tube. These tubes were incubated at 37°C for 1 hour. Urea standards were set up in 2 mL Eppendorf tubes. 1 M urea (0.6 g urea in 10 mL water) was diluted into 50 μL samples from 10 mM to 0.078125 mM in serial dilutions. There was one 50 μL blank. 800 μL of Stop Solution (10 mL 96% acid H_2SO_4 plus 30 mL 85% acid H_3PO_4 plus 70 mL water) was added to each tube. 50 μL of 9% ISPF (α-isonitrosopropiophenone) was added to each tube. Tubes were vortexed for 10 seconds. Holes were punch in the lids. The tubes were heated for 30 minutes at 95°C. Tubes were cooled for 10 minutes on ice. 100 μL of each sample were plated into a new 96-well titer plate with duplicates of each sample. Two rows were allocated for standards. 100 μL of the standards and blanks went into the standard row. The plate was then read at 540 nm on a PowerWave XS Microplate Scanning Spectrophotometer by Bio-Tek® Instruments, Inc. (Winooski, VT). The results were tabulated in Prism 4.0c by GraphPad Software, Inc. (San Diego, CA).

References

Alarcón, R., Orellana, M. S., Neira, B., Uribe, E., García, J. R., & Carvajal, N. (2006). Mutational analysis of substrate recognition by human arginase type I—agmatinase activity of the N130D variant. *FEBS J.*, *273*, 5625–5631.

Albina, J. E., Mills, C. D., Henry, W. L. Jr, & Caldwell, M. D. (1990). Temporal expression of different pathways of 1-arginine metabolism in healing wounds. *J. Immunol.*, *144*(10), 3877–3880.

Anthony, R. M., Rutitzky, L. I., Urban, J. F. Jr., Stadecker, M. J., & Gause, W. C. (2007). Protective immune mechanisms in helminth infection. *Nat. Rev. Immunol.*, *7*, 975–987.

Azenabor, A. A., Kennedy, P., & York, J. (2009). Free intracellular Ca^{2+} regulates bacterial lipopolysaccharide induction of iNOS in human macrophages. *Immunobiology*, *214*, 143–152.

Bogdan, C. (1997). Of microbes, macrophages and nitric oxide. *Behring-Inst.-Mitt.*, *99*, 58–72.

Boucher, J.-L., Custot, J., Vadon, S., Delaforge, M., Lepoivre, M., Tenu, J.-P., Yapo, A., & Mansuy, D. (1994). N^{ω}-hydroxy-L-arginine, an intermediate in the L-arginine to Nitric Oxide pathway, is a strong inhibitor of liver and macrophage Arginase. *Biochem. Biophys. Res. Commun.*, *203*, 1614–1621.

Boucher, J. L., Moali, C., & Tenu, J. P. (1999). Nitric oxide biosynthesis, nitric oxide synthase inhibitors and arginase competition for L-arginine utilization. *Cell. Mol. Life Sci.*, *55*, 1015–1028.

Daghigh, F., Fukuto, J. M., & Ash, D. E. (1994). Inhibition of rat liver Arginase by an intermediate in NO biosynthesis, N^{G}-hydroxy-L-arginine: implications for the regulation of nitric oxide biosynthesis by arginase. *Biochem. Biophys. Res. Commun.*, *202*, 174–180.

Daley, J. M., Brancato, S. K., Thomay, A. A., Reichner, J. S., & Albina, J. E. (2010). The phenotype of murine wound macrophages. *J. Leukoc. Biol.*, *87*(1), 59–67.

El Kasmi, K. C., Qualls, J. E., Pesce, J. T., Smith, A. M., Thompson, R. W., Henao-Tamayo, M., Basaraba, R. J., König, T., Schleicher, U., Koo, M. S., Kaplan, G., Fitzgerald, K. A., Tuomanen, E. I., Orme, I. M., Kanneganti, T. D., Bogdan, C., Wynn, T. A., & Murray, P. J. (2008). Toll-like receptor-induced arginase 1 in macrophages thwarts effective immunity against intracellular pathogens. *Nat. Immunol.*, *9*(12), 1399–1406.

El-Gayar, S., Thuring-Nahler, H., Pfeilschifter, J., Rollinghoff, M., & Bogdan, C. (2003). Translational control of inducible nitric oxide synthase by IL-13 and arginine availability in inflammatory macrophages. *J. Immunol.*, *171*(9), 4561–4568.

Fallon, P. G., & Mangan, N. E. (2007). Suppression of TH2-type allergic reactions by helminth infection. *Nat. Rev. Immunol.*, *7*, 220–230.

Gause, W. C., Urban, J. F. Jr., & Stadecker, M. J. (2003). The immune response to parasitic helminths: insights from murine models. *Trends Immunol.*, *24*, 269–277.

Goldsby, R. A., Kindt, T. J., & Osborne, B. A. (2002). *Kuby immunology* (4th ed.). New York: Freeman.

Gordon, S. (2003). Alternative activation of macrophages. *Nat. Rev. Immunol.*, *3*, 23–35.

Gordon, S. (2007). The macrophage: past, present and future. *Eur. J. Immunol.*, *37*(1), S9–S17.

Gordon, S., & Martinez, F. O. (2010). Alternative activation of macrophages: mechanism and functions. *Immunity*, *32*(5), 593–604.

Gotoh, T., & Mori, M. (1999). Arginase II downregulates nitric oxide (NO) production and prevents NO-mediated apoptosis in murine macrophage-derived RAW 264.7 cells. *J. Cell Biol.*, *144*, 427–434.

Gray, M. J., Poljakovic, M., Kepka-Lenhart, D., & Morris, S. M. Jr. (2005). Induction of arginase I transcription by IL-4 requires a composite DNA response element for STAT6 and C/EBPbeta. *Gene*, *353*, 98–106.

Hecker, M., Nematollahi, H., Hey, C., Busse, R., & Racké, K. (1995). Inhibition of arginase by N^{G}-hydroxy-L-arginine in alveolar macrophages: implications for the utilization of L-arginine for nitric oxide synthesis. *FEBS Lett.*, *359*, 251–254.

Herald, M. C. (2010). General model of inflammation. *Bull. Math. Biol.*, *72*(4), 765–779.

Herbert, D. R., Holscher, C., Mohrs, M., Arendse, B., Schwegmann, A., Radwanska, M., Leeto, M., Kirsch, R., Hall, P., Mossmann, H., Claussen, B., Forster, I., & Brombacher, F. (2004). Alternative macrophage activation is essential for survival during schistosomiasis and down modulates T helper 1 responses and immunopathology. *Immunity*, *20*, 623–635.

Hesse, M., Cheever, A. W., Jankovic, D., & Wynn, T. A. (2000). NOS-2 mediates the protective anti-inflammatory and antifibrotic effects of the Th1-inducing adjuvant, IL-12, in a Th2 model of granulomatous disease. *Am. J. Pathol.*, *157*(3), 945–955.

Hesse, M., Modolell, M., La Flamme, A. C., Schito, M., Fuentes, J. M., Cheever, A. W., Pearce, E. J., & Wynn, T. A. (2001). Differential regulation of nitric oxide synthase-2 and arginase-1 by type1/type2 cytokines in vivo: granulomatous pathology is shaped by the pattern of L-arginine metabolism. *J. Immunol.*, *167*, 6533–6544.

Janeway, C. A., Travers, P., Walport, M., & Shlomichik, M. (2001). *Immunobiology* (Vol. 5). New York: Garland.

Khallou-Laschet, J., Varthaman, A., Fornasa, G., Compain, C., Gaston, A.-T., Clement, M., Cussiot, M., Levillain, O., Graff-Dubois, S., Nicoletti, A., & Caligiuri, G. (2010). Macrophage plasticity in experimental atherosclerosis. *PLoS ONE*, *5*(1), e8852.

Kolodziejski, P. J., Koo, J.-S., & Eissa, N. T. (2004). Regulation of inducible nitric oxide synthase by rapid cellular turnover and cotranslational down-regulation by dimerization inhibitors. *Proc. Natl. Acad. Sci. USA*, *101*(52), 18141–18146.

Krieg, A. M. (2000). Signal transduction induced by immunostimulatory CpG DNA. *Springer Semin. Immunopath*, *22*(1–2), 97–105.

Loehning, M., Hegazy, A. N., Pinschewer, D. D., Busse, D., Lang, K. S., Hofer, T., Radbruch, A., Sinkernagel, R. M., & Hengartner, H. (2008). Long-lived virus-reactive memory T cells generated from purified cytokine-secreting T helper type 1 and type 2 effectors. *J. Exp. Med.*, *205*(1), 53–61.

MacMicking, J., Xie, Q. W., & Nathan, C. (1997). Nitric oxide and macrophage function. *Annu. Rev. Immunol.*, *15*, 323–350.

Maggelakis, S. A. (2003). A mathematical model of tissue replacement during epidermal wound healing. *Appl. Math. Model.*, *27*(3), 189–196.

Maggelakis, S. A. (2004). Modeling the role of angiogenesis in epidermal wound healing. *Discrete Contin. Dyn. Syst., Ser. B*, *4*(1), 267–273.

Mahoney, E., Reichner, J., Bostom, L. R., Mastrofrancesco, B., Henry, W., & Albina, J. (2002). Bacterial colonization and the expression of inducible nitric oxide synthase in murine wounds. *Am. J. Pathol.*, *161*(6), 2143–2152.

Mansuy, D., & Boucher, J.-L. (2004). Alternative nitric oxide-producing substrates for NO synthases. *J. Free Radic. Biol. Med.*, *37*(8), 1105–1121.

Marée, A. F., Komba, M., Dyck, C., Labecki, M., Finegood, D. T., & Edelstein-Keshet, L. (2005). Quantifying macrophage defects in type 1 diabetes. *J. Theor. Biol.*, *233*(4), 533–551.

Marino, S., Myers, A., Flynn, J. L., & Kirschner, D. E. (2010). TNF and IL-10 are major factors in modulation of the phagocytic cell environment in lung and lymph node in tuberculosis: a next-generation two-compartmental model. *J. Theor. Biol.*, *265*(4), 586–598.

Martinez, F. O., Sica, A., Mantovani, A., & Locati, M. (2008). Macrophage activation and polarization. *Front. Biosci.*, *13*, 453–461.

Moali, C., Boucher, J.-L., Sari, M.-A., Stuehr, D. J., & Mansuy, D. (1998). Substrate specificity of NO synthases: detailed comparison of L-arginine, Homo-L-arginine, their N^{ω}-hydroxy derivatives, and N^{ω}-hydroxynor-L-arginine. *Biochemistry*, *37*, 10453–10460.

Moali, C., Brollo, M., Custot, J., Sari, M., Boucher, J.-L., Stuehr, D. J., & Mansuy, D. (2000). Recognition of α-amino acids bearing various C=NOH functions by nitric oxide synthase involves very different structural determinants. *Biochemistry*, *39*, 8208–8218.

Modolell, M., Corraliza, I. M., Link, F., Soler, G., & Eichmann, K. (1995). Reciprocal regulation of the nitric oxide synthase/arginase balance in mouse bone marrow-derived macrophages by TH1 and TH2 cytokines. *Eur. J. Immunol.*, *25*(4), 1101–1104.

Morris, S. M. Jr., Kepka-Lenhart, D., & Chen, L. C. (1998). Differential regulation of arginases and inducible nitric oxide synthase in murine macrophage cells. *Am. J. Physiol.*, *275*(5 Pt 1), E740–E747.

Mosser, D. M. (2003). The many faces of macrophage activation. *J. Leukoc. Biol.*, *73*, 209–212.

Mosser, D. M., & Edwards, J. P. (2008). Exploring the full spectrum of macrophage activation. *Nat. Rev. Immunol.*, *8*(12), 958–969.

Munder, M., Eichmann, K., & Modolell, M. (1998). Alternative metabolic states in murine macrophages reflected by the nitric oxide synthase/arginase balance: competitive regulation by CD4+ T cells correlates with Th1/Th2 phenotype. *J. Immunol.*, *160*, 95347.

Nathan, C. (1994). Nitric oxide and biopterin: a study in Chairoscuro. *J. Clin. Invest.*, *93*(5), 2236–2243.

Ourgrinovskaia, A., Thompson, R. S., & Myerscough, M. R. (2010). An ODE model of early stages of atherosclerosis: mechanisms of the inflammatory response. *Bull. Math. Biol.*, *72*(6), 1534–1561.

Pauleau, A.-L., Rutschman, R., Lang, R., Pernis, A., Watowich, S. S., & Murray, P. J. (2004). Enhancer-mediated control of macrophage-specific arginase I expression. *J. Immunol.*, *172*, 7565–7573.

Pearce, E. J., & MacDonald, A. S. (2002). The immunobiology of schistosomiasis. *Nat. Rev. Immunol.*, *2*(7), 499–511.

Pesce, J., Kaviratne, M., Ramalingam, T. R., Thompson, R. W., Urban, J. F. Jr., Cheever, A. W., Young, D. A., Collins, M., Grusby, M. J., & Wynn, T. A. (2006). The IL-21 receptor augments Th2 effector function and alternative macrophage activation. *J. Clin. Invest.*, *116*(7), 2044–2055.

Pettet, G. J., Byrne, H. M., Mcelwain, D. L. S., & Norbury, J. (1996). A model of wound-healing angiogenesis in soft tissue. *Math. Biosci.*, *136*(1), 35–63.

Porcheray, F., Viaud, S., Rimaniol, A. C., Leone, C., Samah, B., Dereuddre-Bosquet, N., Dormont, D., & Gras, G. (2005). Macrophage activation switching: an asset for the resolution of inflammation. *Clin. Exp. Immunol.*, *142*, 481–489.

Reyes, J. L., & Terrazas, L. I. (2007). The divergent roles of alternatively activated macrophages in helminthic infections. *Parasite Immunol.*, *29*, 609–619.

Rutschman, R., Lang, R., Hesse, M., Ihle, J. N., Wynn, T. A., & Murray, P. J. (2001). Cutting edge: Stat6-dependent substrate depletion regulates nitric oxide production. *J. Immunol.*, *166*(4), 2173–2177.

Santhanam, L., Christianson, D. W., Nyham, D., & Berkowitz, D. E. (2008). Arginase and vascular aging. *J. Appl. Physiol.*, *105*, 1632–1642.

Schreiber, R. D. (1984). Identification of gamma-interferon as a murine macrophage-activating factor for tumor cytotoxicity. *Contemp. Top. Immunobiol*, *13*, 171–198.

Shin, D.-G., Kazmi, S. A., Pei, B., Kim, Y.-A., Maddox, J., Nori, R., Wong, A., Krueger, W., & Rowe, D. (2009). Computing consistency between microarray data and known gene regulation relationships. *IEEE Trans. Inf. Technol. Biomed.*, *13*(6), 1075–1082.

Stadecker, M. J., Asahi, H., Finger, E., Hernandez, H. J., Rutitzky, L. I., & Sun, J. (2004). The immunobiology of Th1 polarization in high-pathology schistosomiasis. *Immunol. Rev.*, *201*, 168–179.

Stein, M., Keshav, S., Harris, N., & Gordon, S. (1992). Interleukin 4 potently enhances murine macrophage mannose receptor activity: a marker of alternative immunologic macrophage activation. *J. Exp. Med.*, *176*(1), 287–292.

Stout, R. D., & Suttles, J. (2004). Functional plasticity of macrophages: reversible adaptation to changing microenvironments. *J. Leukoc. Biol.*, *76*, 509–513.

Stuehr, D. J. (1999). Mammalian nitric oxide synthases. *Biochim. Biophys. Acta*, *1411*, 217–230.

Waugh, H. V., & Sherratt, J. A. (2006). Macrophage dynamics in diabetic wound healing. *Bull. Math. Biol.*, *68*(1), 197–207.

Wei, L. H., Jacobs, A. T., Morris, S. M. Jr., & Ignarro, L. J. (2000). IL-4 and IL-13 up-regulate arginase I expression by cAMP and JAK/STAT6 pathways in vascular smooth muscle cells. *Am. J. Physiol., Cell Physiol.*, *279*, 248–256.

Wendelsdorf, K., Bassaganya-Riera, J., Hontecillas, R., & Eubank, S. (2010). Model of colonic inflammation: immune modulatory mechanisms in inflammatory bowel disease. *J. Theor. Biol.*, *264*(4), 1225–1239.

Wu, G., & Morris, S. M. Jr. (1998). Arginine metabolism: nitric oxide and beyond. *Biochem. J.*, *336*, 1–17.

Xaus, J., Comalada, M., Valledor, A. F., Lloberas, J., López-Soriano, F., Argilés, J. M., Bogdan, C., & Celada, A. (2000). LPS induces apoptosis in macrophages mostly through the autocrine production of TNF-alpha. *Blood*, *95*(12), 3823–3831.